

# Charge state regulation of nuclear excitation by electron capture in $^{229}\text{Th}$ ions\*

Yang-Yang Xu,<sup>1</sup> Qiong Xiao,<sup>1</sup> Jun-Hao Cheng,<sup>1</sup> Wen-Yu Zhang,<sup>1</sup> and Tong-Pu Yu<sup>1,†</sup>

<sup>1</sup>College of Science, National University of Defense Technology, 410073 Changsha, People's Republic of China

Nuclear excitation by electron capture (NEEC) in  $^{229}\text{Th}$  holds significant potential for precise nuclear state manipulation. In this study, we thoroughly investigate NEEC in  $^{229}\text{Th}^{q+}$  ions by integrating quantum numbers  $(n, l, j)$  effects and analyzing key parameters (e.g., resonance energy  $E_r$ , cross section  $\sigma$ , resonance strength  $S$ , and NEEC transition width  $\Gamma_{\text{NEEC}}$ ) influences across charge state from  $q = 1^+$  to  $90^+$ . Especially, we focus on the charge-state regulation of the isomeric state (IS, 8.36 eV) and second-excited state (SE, 29.19 keV). Our calculations uncover critical charge-state-dependent behaviors of NEEC in  $^{229}\text{Th}$  ions: (1) For the IS, valid NEEC channels exhibit threshold migration, where the dominant principal quantum number  $n$  increases linearly with  $q$  following the relation  $n \approx 1.28q + 4.23$ ; meanwhile, single- $n$ -channel  $S$  stabilizes between  $10^{-2}$  to  $10^0$  barn eV via compensatory nucleus-electron coupling, ensuring the total resonance  $S$  constant. (2) For the SE, its excitation energy far exceeds nearly all electron binding energies, leading to negligible channel screening and causing the total  $S$  to increase monotonically with  $q$ . This research clarifies the intrinsic mechanisms of charge-state-driven nuclear-electronic interactions in  $^{229}\text{Th}^{q+}$  NEEC and provides a critical reference for future experimental efforts to manipulate  $^{229}\text{Th}$  nuclear states, particularly via indirect regulation of the SE.

Keywords:  $^{229}\text{Th}^{q+}$ , Nuclear excitation by electron capture, Charge state regulation

## I. INTRODUCTION

The nucleus of  $^{229}\text{Th}$  has long stood out in low-energy nuclear physics and precision spectroscopy due to its unique low-lying isomeric state (IS), with an excitation energy of approximately 8.35574(3) eV above the ground state [1]. This is the lowest known nuclear excited state to date, bridging the traditionally distinct realms of nuclear physics (e.g., nuclear structure, excitation energies) and atomic physics (e.g., electron binding, charge-state effects) [2–6]. Such a peculiar property makes  $^{229}\text{Th}$  a prime candidate for next-generation nuclear optical clocks [7, 8], a sensitive probe for testing fundamental constant variations [9–12], and a platform for exploring nuclear-laser interactions [13–19].

To harness these applications, efficient and controllable population of the  $^{229}\text{Th}$  isomeric state is paramount. Early approaches relied on natural decay processes, such as the  $\alpha$  decay of  $^{233}\text{U}$  [20, 21] or the  $\beta$  decay of  $^{229}\text{Ac}$  [22]. However, these methods suffer from low yields, fixed branching ratios, and uncontrollable recoil energies, limiting their practicality. Alternative strategies, including direct laser excitation and indirect pumping via the 29189.93(0.07) eV second-excited state (SE), have been attempted, but they face challenges such as inefficient coupling between photons and nuclear states or narrow resonance conditions that are difficult to satisfy experimentally [23, 24].

Against this backdrop, nuclear excitation by electron capture (NEEC) has emerged as a promising mechanism for populating nuclear isomers. Proposed almost half a century ago [25], NEEC describes a resonant process where a free electron is captured into an atomic orbital, with the released energy selectively exciting the nucleus to a higher energy state.

It is effectively the time-reversed counterpart of internal conversion (IC) [26, 27]. Theoretically, NEEC offers advantages such as tunable resonance energies and potentially high excitation cross sections [28–39], making it a viable candidate for controlled isomer excitation. Despite its potential, experimental verification of NEEC remains elusive and controversial. The 2018 claim of observing NEEC in  $^{93\text{m}}\text{Mo}$  sparked intense debate [40], as subsequent theoretical calculations showed a discrepancy of up to nine orders of magnitude with the reported signal strength [41]. Follow-up experiments using isomer beams failed to reproduce the effect [42], highlighting the need for more rigorous theoretical frameworks and optimized experimental designs to clarify the NEEC process.

In the specific context of  $^{229}\text{Th}$ , NEEC's role in exciting the isomeric state remains largely unexplored. Previous studies have focused on electronic bridge (EB) [43–50], electron transition (NEET) [51–54], inelastic electron scattering (NEIES) [55–58], or laser-driven recollision processes [5, 6], but the potential of NEEC, particularly its dependence on charge states, electron configurations and resonance conditions, has not been systematically addressed. Key questions persist: How does varying charge states of  $^{229}\text{Th}$  ions modulate the NEEC efficiency? What are the optimal experimental parameters to observe NEEC-induced isomer excitation in  $^{229}\text{Th}$ ? In this work, we aim to address these unresolved aspects by providing a comprehensive analysis of NEEC in  $^{229}\text{Th}$  ions. By investigating the interplay between charge states, electron capture channels, and nuclear transition energies, we quantify NEEC cross sections and resonance strengths under various conditions. Our results clarify certain microscopic mechanisms of nuclear-electron coupling in  $^{229}\text{Th}$  and provide specific references for experimental attempts to verify NEEC, which may contribute to understanding this process and its potential in manipulating the  $^{229}\text{Th}$  isomeric state.

This article is structured as follows. The next section outlines the theoretical framework for NEEC calculations. In

\* This work was supported by the National Natural Science Foundation of China (Grant No.12135009, 12375244), the Natural Science Foundation of Hunan Province of China (Grant No.2025JJ30002), and the Innovation Foundation for Postgraduate (Grant No.XJQY2024046, XJJ2024063).

† Corresponding author, [tongpu@nudt.edu.cn](mailto:tongpu@nudt.edu.cn)

Section III, the detailed results and discussions on the roles of quantum numbers and charge states are provided. In Section IV, we provide a brief summary.

## II. THEORETICAL FRAMEWORK

To quantitatively describe the excitation of the  $^{229}\text{Th}$  nucleus to its excited state (IS and SE) via NEEC, we establish a theoretical framework centered on the interaction between free electrons and the nucleus, where the electron is captured into a bound state while transferring energy to excite the nucleus.

The core of NEEC lies in the coupling between the electron and the nucleus, mediated by both electromagnetic currents and Coulomb interactions. The interaction Hamiltonian  $H_{\text{int}}$  is expressed as [59]

$$H_{\text{int}} = -\frac{1}{c} \int [\mathbf{j}_n(\mathbf{r}) + \mathbf{j}_e(\mathbf{r})] \cdot \mathbf{A}(\mathbf{r}) d\tau + \int \frac{\rho_n(\mathbf{r})\rho_e(\mathbf{r}')}{|\mathbf{r} - \mathbf{r}'|} d\tau d\tau'. \quad (1)$$

Here, the first term describes the coupling between nuclear current density  $\mathbf{j}_n(\mathbf{r})$  and electron current density  $\mathbf{j}_e(\mathbf{r})$  via the radiation field's vector potential  $\mathbf{A}(\mathbf{r})$ . The second term accounts for the Coulomb interaction between nuclear charge density  $\rho_n(\mathbf{r})$  and electron charge density  $\rho_e(\mathbf{r}')$ .

For the electronic states involved in NEEC, the initial state is a free electron with kinetic energy  $E_i$ , and the final state is a bound atomic orbital with energy  $E_f$ . Energy conservation requires  $E_i = \Delta E + |E_f|$ , where  $\Delta E$  is the energy difference between the final and initial nuclear states. Electron wavefunctions are solutions to the Dirac equation under the Dirac-Hartree-Fock-Slater (DHFS) potential [60]

$$V_{\text{DHFS}}(r) = V_n(r) + V_e(r) + V_{\text{ex}}(r), \quad (2)$$

where the nuclear potential  $V_n(r)$  arises from a Fermi-distributed nuclear charge density [61], the electronic potential  $V_e(r)$  from the electron cloud, and the exchange potential  $V_{\text{ex}}(r)$  from a piecewise Thomas-Fermi approximation for exchange interactions [62].

The NEEC cross section, which quantifies the probability of the process, is given by

$$\begin{aligned} \sigma_{\text{E(M)}\lambda} &= \frac{4\pi^2}{c^2} \frac{E_i + c^2}{p_i^3} \times \sum_{l_i, j_i, l_f, j_f} \frac{\kappa^{2\lambda+2}}{(2\lambda-1)!!^2} \\ &\times \frac{(2l_i+1)(2l_f+1)(2j_i+1)(2j_f+1)}{(2\lambda+1)^2} \\ &\times \left( \begin{matrix} l_f & l_i & \lambda \\ 0 & 0 & 0 \end{matrix} \right)^2 \left\{ \begin{matrix} l_i & \lambda & l_f \\ j_f & 1/2 & j_i \end{matrix} \right\}^2 |T_{fi}^{\text{E(M)}\lambda}|^2 \\ &\times B(\text{E(M)}\lambda, I_i \rightarrow I_f) \frac{\Gamma_{\text{NEEC}}}{\Delta E^2 + \Gamma_{\text{NEEC}}^2/4}. \end{aligned} \quad (3)$$

In this expression, E and M denote electric and magnetic

multipole transitions, respectively, with  $\lambda$  indicating the order of the multipole, while  $B(\text{E(M)}\lambda, I_i \rightarrow I_f)$  represents the reduced nuclear transition probability that encapsulates the intrinsic strength of the nuclear transition.  $\kappa = E_{\text{exc}}/c$  with  $E_{\text{exc}}$  being the excitation energy and  $T_{fi}^{\text{E(M)}\lambda}$  are the radial matrix elements that quantify the overlap between the initial and final electronic wavefunctions, a critical factor in determining transition probabilities.  $\Gamma_{\text{NEEC}}$  represents the total transition width, which is the sum of  $\Gamma_{\text{spont}}$  and  $\Gamma_n$ .  $\Gamma_{\text{spont}}$  corresponds to the spontaneous emission width of the final electronic state, reflecting the probability of the electron transitioning to lower energy levels through photon emission.  $\Gamma_n$  denotes the nuclear width, which includes  $\Gamma_{\text{IC}}$  (internal conversion width, characterizing the probability of energy transfer from the nucleus to atomic electrons) and  $\Gamma_\gamma$  (gamma decay width, describing the probability of radiative decay via  $\gamma$ -ray emission).

The radial matrix elements  $T_{fi}^{\text{E}\lambda}$  and  $T_{fi}^{\text{M}\lambda}$  are defined as

$$\begin{aligned} T_{fi}^{\text{E}\lambda} &= \int_0^\infty h_\lambda^{(1)}(\kappa r) [g_i(r)g_f(r) + f_i(r)f_f(r)] r^2 dr \\ &- \int_0^\infty h_{\lambda-1}^{(1)}(\kappa r) \frac{\kappa}{\lambda} [g_i(r)g_f(r) + f_i(r)f_f(r)] r^3 dr, \end{aligned} \quad (4)$$

and

$$\begin{aligned} T_{fi}^{\text{M}\lambda} &= \frac{\eta_i + \eta_f}{\lambda} \\ &\times \int_0^\infty h_\lambda^{(1)}(\kappa r) [g_i(r)f_f(r) + g_f(r)f_i(r)] r^2 dr. \end{aligned} \quad (5)$$

Here,  $h^{(1)}(\kappa r)$  is the spherical Hankel function of the first kind, and  $\eta = (l-j)(2j+1)$  with  $l$  replaced by  $l' = 2j-l$  for  $\eta < 0$  or M $\lambda$  transitions.  $g(r)$  and  $f(r)$  denote the radial components of the upper and lower parts of the Dirac spinor [63], respectively, with the subscripts  $i$  and  $f$  corresponding to the initial and final states of the electron.

When the incoming electron energy exhibits a distribution, the resonance strength  $S$  serves to simplify calculations

$$S = \int \sigma_{\text{NEEC}}(E_i) dE_i. \quad (6)$$

All calculations above use atomic units (a.u.) with the reduced Planck constant ( $\hbar$ ) = electron mass ( $m_e$ ) = elementary charge ( $e$ ) = 1. Lengths measured in Bohr radii, energies in Hartrees, and the speed of light given by  $c = 1/\alpha \approx 137.036$  where  $\alpha$  is the fine-structure constant.

## III. RESULTS AND DISCUSSION

In this study, we initiate our exploration of the NEEC process in singly charged thorium ions ( $\text{Th}^{1+}$ ) with the ground-state electronic configuration  $[\text{Rn}]6d^17s^2$ . For the  $^{229}\text{Th}$  nucleus, three primary states exist with distinct spin-parity configurations including the ground state (GS) of  $5/2^+$ , IS of  $3/2^+$ , and SE of  $5/2^+$ . Transitions between the GS and both

excited states adhere to the selection rules governing multipole radiation and parity conservation, allowing them to proceed via magnetic dipole (M1) or electric quadrupole (E2) modes. Theoretical calculations have established the reduced transition probabilities with the IS-to-GS transition exhibiting a  $B(E2)$  value of 27 W.u. and a  $B(M1)$  value of 0.0076 W.u. while the SE-to-GS transition shows a  $B(E2)$  value of 39.49 W.u. and a  $B(M1)$  value of 0.0043 W.u. [64–67]. With this background, we aim to clarify how the principal quantum number ( $n$ ) of the final-state orbit affects the  $\sigma$ ,  $\Gamma_{\text{NEEC}}$  and  $S$ , and to quantify the contributions of M1 and E2 transitions. To this end, we focus on the  $s_{1/2} \rightarrow nd_{3/2}$  channels, as they support both transition types.

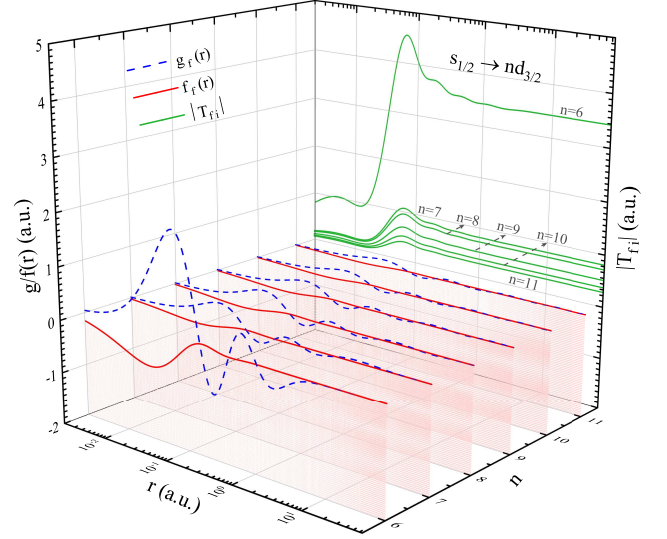


Fig. 2. Radial components of Dirac spinors ( $g(r)$ ,  $f(r)$ ) and transition matrix elements for different final states.

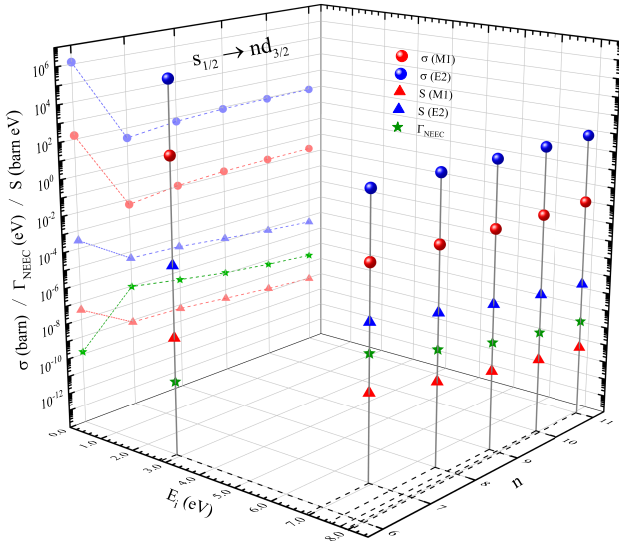


Fig. 1. Three-dimensional visualization of NEEC parameters  $\sigma$ ,  $\Gamma_{\text{NEEC}}$ ,  $S$  ( $z$ -axis) as functions of  $E_i$  ( $x$ -axis) and final-state  $n$  ( $y$ -axis), with projections on the  $y-z$  plane for clarity.

The calculation results are shown in Fig. 1. For systems with spontaneous radiation channels,  $\Gamma_{\text{NEEC}}$  is dominated by  $\Gamma_{\text{spon}}$  as  $\Gamma_{\text{IC}}$  is typically orders of magnitude smaller. This is evident through the abrupt rise in  $\Gamma_{\text{NEEC}}$  between the  $6d_{3/2}$  and  $7d_{3/2}$  states, as observed from projections on the  $y-z$  plane. The  $6d_{3/2}$  state has limited spontaneous radiation channels, with only the E1 transition to  $5f_{5/2}$ , whereas the  $7d_{3/2}$  state possesses five such pathways. As  $n$  increases from 7 to 11, despite more radiative channels becoming available,  $\Gamma_{\text{NEEC}}$  decreases slowly. This trend arises because larger  $n$  pushes the electron orbit further from the nucleus, weakening the electron-nucleus interactions and reducing the probability of spontaneous radiation.

From the cross-section formula Eq. (3), the magnitude of the cross-section peak is jointly determined by  $E_i$ ,  $\Gamma_{\text{NEEC}}$  and  $|T_{fi}|$ , which is inversely proportional to the first two and directly proportional to the square of the latter. The resonance center energy  $E_r$  rises with  $n$  as higher- $n$  orbitals own weaker electron binding energies and thus demand greater initial electron kinetic energy to maintain energy conservation. To identify the primary determinant of the cross-section peak, we also plot the radial components  $g(r)$  and  $f(r)$  and the corresponding  $|T_{fi}|$  for each final state in Fig. 2. With increasing  $n$ , the lower amplitude in the excitation-effective region grows, leading to a smaller  $|T_{fi}|$  that decays distinctly: dropping sharply from  $n=6$  to  $n=7$  and then decreasing much more slowly for  $n \geq 7$ . This pattern aligns with the  $\sigma$  trend in Fig. 1, where the initial decline arises because the large reduction in  $|T_{fi}|$  and the increase in  $\Gamma_{\text{NEEC}}$  outweigh the rising  $E_i$ . For  $n \geq 7$ , the rising  $E_i$  and slower decay of both  $|T_{fi}|$  and  $\Gamma_{\text{NEEC}}$  collectively drive  $\sigma$  to increase. Furthermore, as  $n$  increases,  $S$  shows a stable downward trend. Despite fluctuations in  $\sigma$ , the combined effects of diminishing radial wavefunction overlap and the gradual reduction in  $\Gamma_{\text{NEEC}}$  dominate, resulting in an overall decrease in  $S$ . In terms of transition contributions, E2 transitions play a dominant role, with

their  $\sigma$  and  $S$  far exceeding those of M1 transitions. This disparity arises from transition selection rules and orbital angular momentum characteristics that favor E2 transitions in this channel, making them the primary contributors to the NEEC process.

TABLE 1. The calculation results for NEEC correspond to the E2 transitions of the ground-state  $\text{Th}^{1+}$  with a final-state  $n = 8$ .

Transition	$\sigma$ (barn)	$S$ (barn eV)	$\Gamma_{\text{NEEC}}$ (eV)
$s_{1/2} \rightarrow 8d_{3/2}$	5.84E+01	2.98E-06	3.19E-08
$s_{1/2} \rightarrow 8d_{5/2}$	1.41E-01	7.50E-09	3.33E-08
$p_{1/2} \rightarrow 8p_{3/2}$	7.70E+04	7.44E-04	6.04E-09
$p_{1/2} \rightarrow 8f_{5/2}$	4.69E-03	2.55E-10	3.40E-08
$p_{3/2} \rightarrow 8p_{1/2}$	1.25E+05	7.89E-04	3.94E-09
$p_{3/2} \rightarrow 8p_{3/2}$	4.30E+04	4.16E-04	6.04E-09
$p_{3/2} \rightarrow 8f_{5/2}$	4.75E-04	2.58E-11	3.40E-08
$p_{3/2} \rightarrow 8f_{7/2}$	9.09E-04	4.78E-11	3.28E-08
$d_{3/2} \rightarrow 8s_{1/2}$	8.79E+01	8.45E-06	6.01E-08
$d_{3/2} \rightarrow 8d_{3/2}$	1.65E+02	8.39E-06	3.19E-08
$d_{3/2} \rightarrow 8d_{5/2}$	4.19E+01	2.23E-06	3.33E-08
$d_{5/2} \rightarrow 8s_{1/2}$	8.52E-02	8.19E-09	6.01E-08
$d_{5/2} \rightarrow 8d_{3/2}$	4.47E+01	2.28E-06	3.19E-08
$d_{5/2} \rightarrow 8d_{5/2}$	1.59E+02	8.49E-06	3.33E-08
$f_{5/2} \rightarrow 8p_{1/2}$	1.23E-01	7.72E-10	3.94E-09
$f_{5/2} \rightarrow 8p_{3/2}$	2.91E-04	2.81E-12	6.04E-09
$f_{5/2} \rightarrow 8f_{5/2}$	1.15E+00	6.23E-08	3.40E-08
$f_{5/2} \rightarrow 8f_{7/2}$	1.85E-01	9.71E-09	3.28E-08
$f_{7/2} \rightarrow 8p_{3/2}$	2.78E-02	2.68E-10	6.04E-09
$f_{7/2} \rightarrow 8f_{5/2}$	1.64E-01	8.89E-09	3.40E-08
$f_{7/2} \rightarrow 8f_{7/2}$	1.42E+00	7.46E-08	3.28E-08

To further investigate the influence of the orbital angular momentum  $l$  and total angular momentum  $j$  on the NEEC parameters, we focused on E2 transitions in ground-state  $\text{Th}^{1+}$  with final-state  $n=8$ . The results are presented in Table 1 and visualized in Fig. 3, in which side-plane projections show that  $\sigma$  and  $S$  decrease overall with increasing  $l$ . This arises from reduced radial wavefunction overlap between initial and final states with higher  $l$ . Electron clouds diverge more significantly, suppressing transition probability and attenuating  $\sigma$ . At the microscopic level, transitions with matched  $l$  (e.g.,  $p \rightarrow p$ ,  $f \rightarrow f$ ) exhibit local maxima in  $\sigma$  due to improved symmetry matching, whereas mismatched  $l$  further diminishes the radial wavefunction overlap and  $\sigma$ . Resonance strength  $S$ , jointly determined by  $\sigma$  and  $\Gamma_{\text{NEEC}}$ , closely tracks the trend of  $\sigma$  owing to the modest magnitude of  $\Gamma_{\text{NEEC}}$ 's increase with  $l$ . For fixed  $l$ ,  $\Gamma_{\text{NEEC}}$  exhibits weak sensitivity to  $j$ , with values for transitions sharing the same  $l$  but differing  $j$  remaining within the same order of magnitude. In contrast,  $j$  strongly modulates  $\sigma$ : for example,  $d$ -orbital transitions with different  $j$  exhibit cross-section variations up to three orders of magnitude, underscoring  $j$ 's role in shaping wavefunction overlap with the initial state.

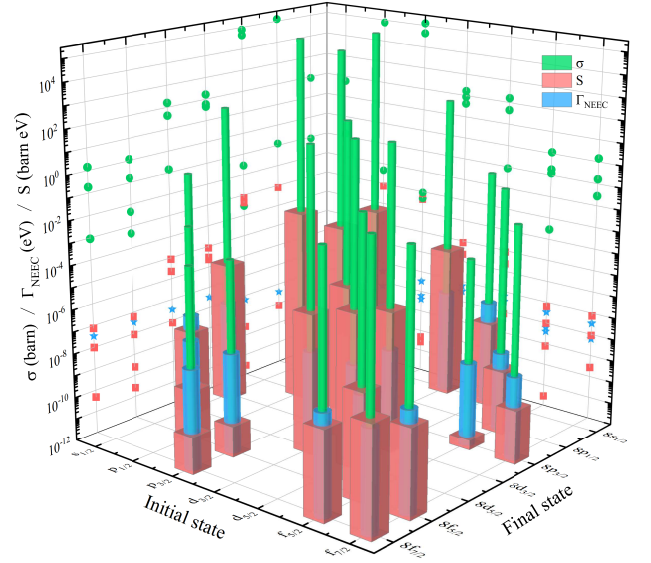


Fig. 3. Three-dimensional visualization of NEEC parameters for ground-state  $\text{Th}^{1+}$ : influence of  $l$  and  $j$  in  $n=8$  transitions (with side-plane projections;  $x/y$ -axes: initial/final states;  $z$ -axis:  $\sigma$ ,  $S$ , and  $\Gamma_{\text{NEEC}}$ ).

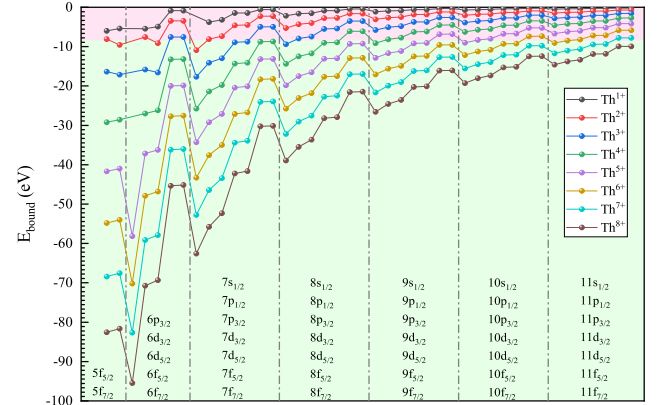


Fig. 4. Binding energy spectrum of electronic holes in  $\text{Th}^{q+}$  across low charge states ( $q = 1^+ \rightarrow 8^+$ ). The pink region indicates valid NEEC channels with  $|E_{\text{bound}}| < 8.36$  eV.

The above results elucidate that quantum numbers constitute the core microscopic parameters governing the activity of NEEC channels, with the regulatory role of the ionic charge state  $q$  manifesting precisely in its capacity to reshape the electronic binding energy spectrum and to screen these quantum numbers. Therefore, we proceed to explore the macroscopic regulation of  $q$ , building on the microscopic insights into quantum numbers. Fig. 4 illustrates the binding energy spectrum of electronic holes in low- $q$  and the pink region denotes valid IS NEEC channels with  $|E_{\text{bound}}| < 8.36$  eV. As  $q$  increases, the strengthened Coulomb potential elevates  $|E_{\text{bound}}|$ , leaving fewer channels within the pink region—a process termed “channel screening”. For instance,  $\text{Th}^{1+}$  sup-



ports nearly all  $5f$  to  $11f$  holes, while  $\text{Th}^{7+}$  retains only high- $n$ , high- $l$  orbitals like  $11f$ . This reduces the number of viable channels, yet the remaining channels exhibit enhanced coupling strength, as revealed by Fig. 5.

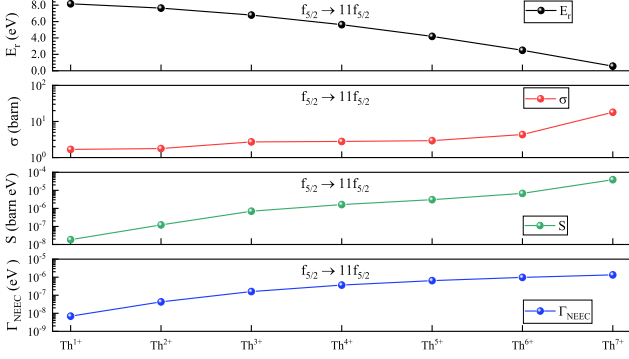


Fig. 5. NEEC parameters ( $E_r$ ,  $\sigma$ ,  $S$ ,  $\Gamma_{\text{NEEC}}$ ) for the  $f_{5/2} \rightarrow 11f_{5/2}$  transition as a function of charge state  $q$ .

Focusing on the surviving  $f_{5/2} \rightarrow 11f_{5/2}$  channel, Fig. 5 details parameter evolution with  $q$ . While  $E_r$  decreases monotonically, consistent with  $E_r = 8.36 - |E_{\text{bound}}|$ ,  $\sigma$  and  $S$  exhibit significant increases. This apparent contradiction is resolved by considering the Coulomb contraction of electron wavefunctions in high- $q$  ions [58]. Despite the large  $n = 11$  and  $l = 3$  values, which would typically disperse the wavefunction, the enhanced Coulomb potential pulls the wavefunction closer to the nucleus, amplifying  $|T_{fi}|$  and thus increasing  $\sigma$ . Concurrently,  $\Gamma_{\text{NEEC}}$  broadens due to stronger spontaneous radiation from tightly bound electrons, driving  $S$  growth via the combined effect of rising  $\sigma$  and  $\Gamma_{\text{NEEC}}$ .

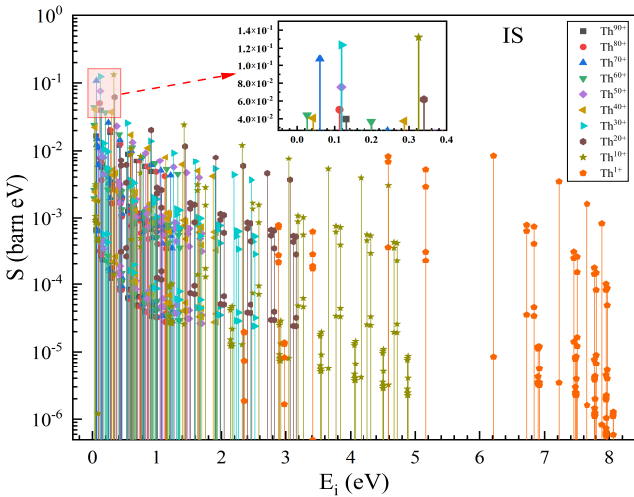


Fig. 6. Multi-channel  $S$  for the IS across charge states. Each color represents a distinct  $\text{Th}^{q+}$  charge state.

To unravel the interplay between charge state and resonance dynamics, we first analyze the IS through its multi-channel behavior and underlying mechanisms. The multi-channel landscape of the IS, visualized in Fig. 6, shows a

key feature across all charge states ( $q=1^+, 10^+, \dots, 90^+$ ): the strongest  $S$  peaks cluster within an  $E_r$  range of 0-0.4 eV, with intensities remaining remarkably consistent. This stability in energy distribution and strength arises from a balance between structural evolution and coupling enhancement.

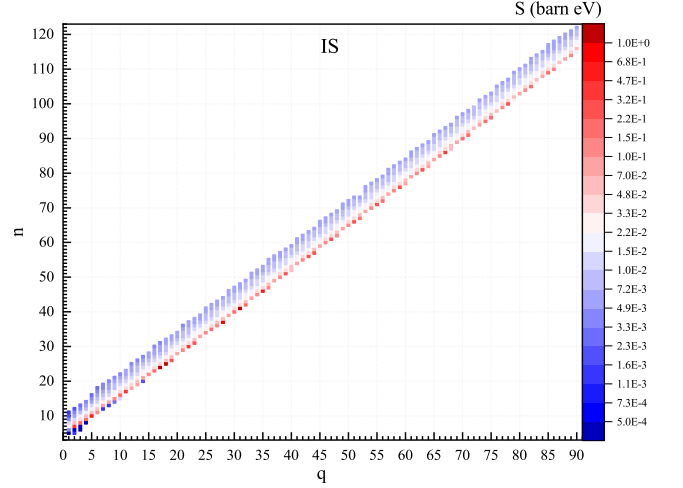


Fig. 7.  $S$  of IS NEEC channels as a function of  $q$  and  $n$ .

Fig. 7 maps  $S$  across  $q$  ( $1^+ \rightarrow 90^+$ ) and  $n$  for the IS, which illustrates a striking threshold migration of valid NEEC channels with increasing  $q$ . At low  $q$  (e.g.,  $q = 1^+$ ), effective channels span a broad range of  $n$ , consistent with the abundant low- $q$  channels observed in Fig. 4. As  $q$  rises, this range shifts monotonically toward higher  $n$  and for  $q = 90^+$ , valid channels are restricted to  $n \leq 115$ . This rigid migration directly arises from the need to maintain the energy-matching condition under a strengthened Coulomb potential—only high- $n$  orbitals, with their weaker binding energies, can satisfy this constraint. Quantitative analysis shows that the dominant  $n$  (the  $n$  contributing the maximum  $S$  for each  $q$ ) follows a linear relationship  $n \approx 1.28q + 4.23$ , confirming Coulomb potential as the key driver of orbital availability for IS. Notably, despite the significant shift in dominant  $n$ , the corresponding maximum  $S$  exhibits remarkable stability across  $q$ , with values clustering between  $10^{-5}$  barn eV and  $10^0$  barn eV. For example,  $q = 9^+$  (dominant  $n=15$ ),  $q = 50^+$  (dominant  $n=65$ ) and  $q = 89^+$  (dominant  $n=114$ ) yield  $S \approx 10^{-1}$  barn eV. This stability results from a compensatory interplay where Coulomb contraction amplifies  $|T_{fi}|$  in high- $n$  orbitals, thereby offsetting the spatial dispersion inherent to larger  $n$  values and balancing the reduced number of available channels with enhanced single-channel coupling strength.

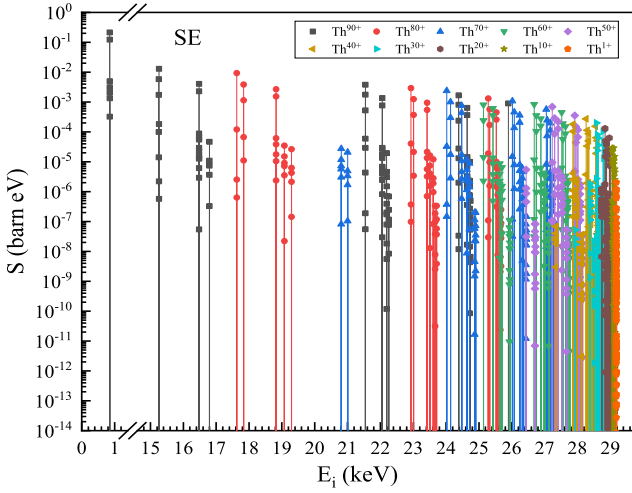


Fig. 8. Multi-channel  $S$  for the SE across charge states. Each color represents a distinct  $\text{Th}^{q+}$  charge state.

Focus shifts to the SE, whose investigation is driven by its substantial role in indirectly populating the IS with approximately 90% of SE decays occurring via transitions to the IS such that a high excitation rate of the SE would result in non-negligible indirect excitation of the IS [23]. The SE exhibits distinct behavior rooted in its unique energetic properties. Fig. 8 structured to mirror Fig. 6 for direct comparison shows two defining trends: maximum  $S$  span a dispersed  $E_r$  range, and their intensities surge with  $q$  while  $E_r$  itself decreases monotonically. These features reflect a liberation from the constraints governing the IS.

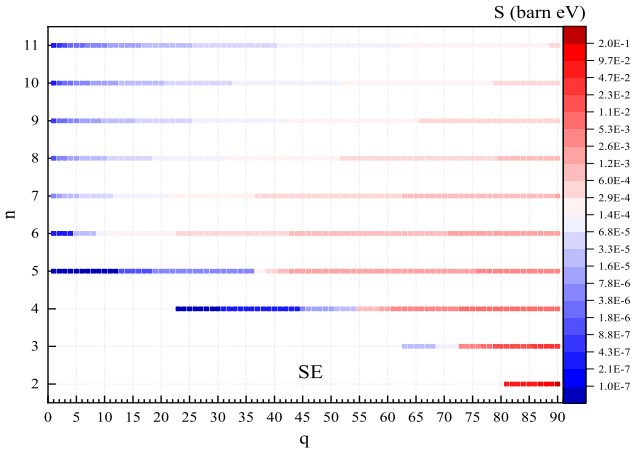


Fig. 9.  $S$  of SE NEEC channels as a function of  $q$  and  $n$ .

Fig. 9 shows the SE exhibits negligible threshold migration with valid channels confined to a narrow  $n$  range ( $n_{i5}$  for low  $q$ , extending to  $n_{i2}$  at  $q = 90^+$ ) across all charge states. This insensitivity occurs because the SE excitation energy (29.19 keV) vastly exceeds electron binding energies for almost all  $q$ , obviating channel screening. Consequently, the maximum  $S$  from the dominant  $n$  for each  $q$  grows monotonically by 4 orders of magnitude (e.g., from  $4.65 \times 10^{-6}$

barn eV at  $q = 1^+$  to  $3.47 \times 10^{-1}$  barn eV at  $q = 90^+$ ), driven solely by Coulomb contraction strengthening electron-nucleus coupling across all  $n$  without countervailing channel loss.

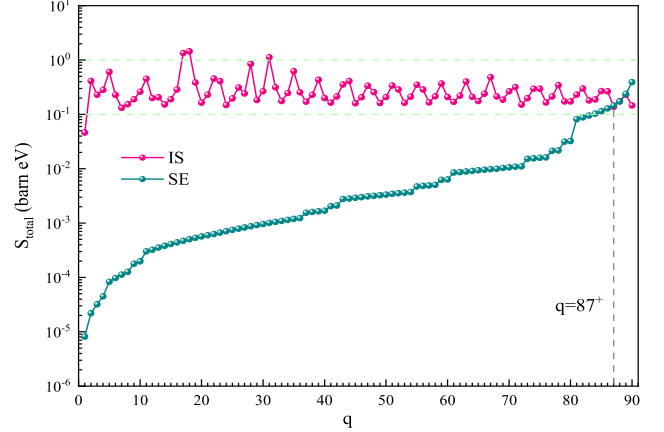


Fig. 10. Total resonance strength  $S_{\text{total}}$  for IS and SE states as a function of charge state  $q$ .

These results reveal  $q$ 's dual role: for low excitation energies (IS), it acts as a channel filter, with coupling enhancement compensating for reduced channel quantity; for high excitation energies (SE), it functions as a coupling amplifier, enabling unconstrained efficiency growth. Finally, global trends in the total resonance strength  $S_{\text{total}}$  are summarized in Fig. 10. As observed, the IS  $S_{\text{total}}$ —reflecting the regulatory balance between threshold migration and compensatory enhancement—remains remarkably stable, fluctuating within the range of  $10^{-1}$  to  $10^0$  barn eV. In contrast, the SE  $S_{\text{total}}$  grows exponentially with  $q$ , surging from  $10^{-6}$  to  $10^1$  barn eV. Notably, these trends intersect at  $q = 87^+$ , beyond which the SE  $S_{\text{total}}$  surpasses that of the IS. Hence, for charge states in the range  $q = 87^+$  to  $90^+$ , indirect population of the IS via regulating the SE's NEEC process is more feasible than direct excitation of the IS, which is limited by the stability of channel screening and coupling compensation. This indirect strategy offers two key advantages: first, it circumvents challenges in direct excitation, such as the migration of IS channels to the hard-to-regulate  $n > 115$  region under high charge states; second, it lowers requirements on the energy precision for lasers or electron beams. Consequently, it provides a practical parameter window for controllable, high-intensity IS population and facilitates parameter optimization in nuclear optical clocks.

#### IV. SUMMARY

Given NEEC's potential for controlling  $^{229}\text{Th}$  nuclear states, this work examines NEEC in  $^{229}\text{Th}^{q+}$  ions with a focus on the effect of quantum numbers  $n, l, j$  and charge states  $q$ . It is shown that quantum numbers exert distinct effects on NEEC key parameters: the resonance strength  $S$  decreases

with increasing  $n$ , larger  $l$  suppresses both  $\sigma$  and  $S$ , and  $j$  weakly affects  $\Gamma_{\text{NEEC}}$  but strongly modulates  $\sigma$ . For the isomeric state, valid channels show threshold migration, with dominant  $n$  increasing linearly with  $q$  and single- $n$ -channel  $S$  stabilizes via compensatory nucleus-electron coupling to keep  $S_{\text{total}}$  constant. For the second excited state,  $S_{\text{total}}$  increases monotonically with  $q$  due to negligible screening.

Furthermore, we find that when  $q \geq 87^+$ , the total resonance strength  $S_{\text{total}}$  of the SE prevails. This not only offers a new experimental path to indirectly populate the IS by regulating the SE but also clarifies charge-state-driven nuclear-electronic interactions, providing insights for the precise manipulation of  $^{229}\text{Th}$  nuclear states.

- 
- [1] J. Tiedau, M. V. Okhapkin, K. Zhang *et al.*, Laser excitation of the Th-229 nucleus. *Phys. Rev. Lett.* **132**, 182501 (2024). doi: [10.1103/PhysRevLett.132.182501](https://doi.org/10.1103/PhysRevLett.132.182501)
  - [2] P. G. Thirolf, S. Kraemer, D. Moritz *et al.*, The thorium isomer  $^{229\text{m}}\text{Th}$ : review of status and perspectives after more than 50 years of research. *Eur. Phys. J. Spec. Top.* **233**, 1113 (2024). doi: [10.1140/epjs/s11734-024-01098-2](https://doi.org/10.1140/epjs/s11734-024-01098-2)
  - [3] M. G. Kozlov, A. V. Oleynikchenko, D. Budker *et al.*, Excitation of the  $^{229\text{m}}\text{Th}$  nucleus by a hole in the inner electronic shells. *Phys. Rev. A* **109**, 042806 (2024). doi: [10.1103/PhysRevA.109.042806](https://doi.org/10.1103/PhysRevA.109.042806)
  - [4] P. V. Bilous, G. A. Kazakov, I. D. Moore *et al.*, Internal conversion from excited electronic states of  $^{229}\text{Th}$  ions. *Phys. Rev. A* **95**, 032503 (2017). doi: [10.1103/PhysRevA.95.032503](https://doi.org/10.1103/PhysRevA.95.032503)
  - [5] W. Wang, J. Zhou, B. Liu *et al.*, Exciting the isomeric  $^{229}\text{Th}$  nuclear state via laser-driven electron recollision. *Phys. Rev. Lett.* **127**, 052501 (2021). doi: [10.1103/PhysRevLett.127.052501](https://doi.org/10.1103/PhysRevLett.127.052501)
  - [6] X. Wang, Nuclear excitation of  $^{229}\text{Th}$  induced by laser-driven electron recollision. *Phys. Rev. C* **106**, 024606 (2022). doi: [10.1103/PhysRevC.106.024606](https://doi.org/10.1103/PhysRevC.106.024606)
  - [7] C. J. Campbell, A. G. Radnaev, A. Kuzmich *et al.*, Single-ion nuclear clock for metrology at the 19th decimal place. *Phys. Rev. Lett.* **108**, 120802 (2012). doi: [10.1103/PhysRevLett.108.120802](https://doi.org/10.1103/PhysRevLett.108.120802)
  - [8] P. G. Thirolf, B. Seiferle, L. von der Wense, The 229-thorium isomer: doorway to the road from the atomic clock to the nuclear clock. *J. Phys. B At. Mol. Opt. Phys.* **52**, 203001 (2019). doi: [10.1088/1361-6455/ab29b8](https://doi.org/10.1088/1361-6455/ab29b8)
  - [9] W. G. Rellergert, D. DeMille, R. R. Greco *et al.*, Constraining the evolution of the fundamental constants with a solid-state optical frequency reference based on the  $^{229}\text{Th}$  nucleus. *Phys. Rev. Lett.* **104**, 200802 (2010). doi: [10.1103/PhysRevLett.104.200802](https://doi.org/10.1103/PhysRevLett.104.200802)
  - [10] V. V. Flambaum, Enhanced effect of temporal variation of the fine structure constant and the strong interaction in  $^{229}\text{Th}$ . *Phys. Rev. Lett.* **97**, 092502 (2006). doi: [10.1103/PhysRevLett.97.092502](https://doi.org/10.1103/PhysRevLett.97.092502)
  - [11] J. C. Berengut, V. A. Dzuba, V. V. Flambaum *et al.*, Proposed experimental method to determine  $\alpha$  sensitivity of splitting between ground and 7.6 eV isomeric states in  $^{229}\text{Th}$ . *Phys. Rev. Lett.* **102**, 210801 (2009). doi: [10.1103/PhysRevLett.102.210801](https://doi.org/10.1103/PhysRevLett.102.210801)
  - [12] P. Fadeev, J. C. Berengut, V. V. Flambaum, Sensitivity of  $^{229}\text{Th}$  nuclear clock transition to variation of the fine-structure constant. *Phys. Rev. A* **102**, 052833 (2020). doi: [10.1103/PhysRevA.102.052833](https://doi.org/10.1103/PhysRevA.102.052833)
  - [13] F. F. Karpeshin, Laser assisted two-photon electron-nucleus resonance as applied to producing the  $^{229\text{m}}\text{Th}$  isomer. *Phys. Rev. C* **110**, 054307 (2024). doi: [10.1103/PhysRevC.110.054307](https://doi.org/10.1103/PhysRevC.110.054307)
  - [14] X. J. Liu, Triggering highly nonlinear responses in  $^{229}\text{Th}$  nuclei with an intense laser. *Nucl. Sci. Tech.* **36**, 20 (2025). doi: [10.1007/s41365-024-01632-w](https://doi.org/10.1007/s41365-024-01632-w)
  - [15] A. V. Andreev, A. B. Savelev, S. Y. Stremoukhov *et al.*, Nuclear isomer excitation in  $^{229}\text{Th}$  atoms by superintense laser fields. *Phys. Rev. A* **99**, 013422 (2019). doi: [10.1103/PhysRevA.99.013422](https://doi.org/10.1103/PhysRevA.99.013422)
  - [16] E. V. Tkalya, Proposal for a Nuclear Gamma-Ray Laser of Optical Range. *Phys. Rev. Lett.* **106**, 162501 (2011). doi: [10.1103/PhysRevLett.106.162501](https://doi.org/10.1103/PhysRevLett.106.162501)
  - [17] J. Qi, H. Zhang, X. Wang, Isomeric excitation of  $^{229}\text{Th}$  in laser-heated clusters. *Phys. Rev. Lett.* **130**, 112501 (2023). doi: [10.1103/PhysRevLett.130.112501](https://doi.org/10.1103/PhysRevLett.130.112501)
  - [18] J. Qi, B. Liu, X. Wang, Laser-based approach to verify nuclear excitation by electron capture. *Phys. Rev. C* **110**, L051601 (2024). doi: [10.1103/PhysRevC.110.L051601](https://doi.org/10.1103/PhysRevC.110.L051601)
  - [19] K. A. Tanaka, K. M. Spohr, D. L. Balabanski *et al.*, Current status and highlights of the ELI-NP research program. *Matter Radiat. Extremes* **5**, 024402 (2020). doi: [10.1063/1.5093535](https://doi.org/10.1063/1.5093535)
  - [20] B. R. Beck, J. A. Becker, P. Beiersdorfer *et al.*, Energy Splitting of the Ground-State Doublet in the Nucleus  $^{229}\text{Th}$ . *Phys. Rev. Lett.* **98**, 142501 (2007). doi: [10.1103/PhysRevLett.98.142501](https://doi.org/10.1103/PhysRevLett.98.142501)
  - [21] S. Stellmer, M. Schreitl, G. A. Kazakov *et al.*, Feasibility study of measuring the  $^{229}\text{Th}$  nuclear isomer transition with  $^{233}\text{U}$ -doped crystals. *Phys. Rev. C* **94**, 014302 (2016). doi: [10.1103/PhysRevC.94.014302](https://doi.org/10.1103/PhysRevC.94.014302)
  - [22] M. Verlinde, S. Kraemer, J. Moens *et al.*, Alternative approach to populate and study the  $^{229}\text{Th}$  nuclear clock isomer. *Phys. Rev. C* **100**, 024315 (2019). doi: [10.1103/PhysRevC.100.024315](https://doi.org/10.1103/PhysRevC.100.024315)
  - [23] T. Masuda, A. Yoshimi, A. Fujieda *et al.*, X-ray pumping of the  $^{229}\text{Th}$  nuclear clock isomer. *Nature* **573**, 238-342 (2019). doi: [10.1038/s41586-019-1542-3](https://doi.org/10.1038/s41586-019-1542-3)
  - [24] C. J. Yang, K. M. Spohr, M. O. Cernaianu *et al.*, A new scheme for isomer pumping and depletion with high-power lasers. *Matter Radiat. Extremes* **10**, 057201 (2025). doi: [10.1063/5.0251667](https://doi.org/10.1063/5.0251667)
  - [25] V. Goldanskii, V. Namiot, On the excitation of isomeric nuclear levels by laser radiation through inverse internal electron conversion. *Phys. Lett. B* **62**, 393-394 (1976). doi: [10.1016/0370-2693\(76\)90665-1](https://doi.org/10.1016/0370-2693(76)90665-1)
  - [26] B. Seiferle, L. von der Wense, P. G. Thirolf, Lifetime measurement of the  $^{229}\text{Th}$  nuclear isomer. *Phys. Rev. Lett.* **118**, 042501 (2017). doi: [10.1103/PhysRevLett.118.042501](https://doi.org/10.1103/PhysRevLett.118.042501)
  - [27] E. V. Tkalya, R. Si, Internal conversion of the low-energy  $^{229\text{m}}\text{Th}$  isomer in the thorium anion. *Phys. Rev. C* **101**, 054602 (2020). doi: [10.1103/PhysRevC.101.054602](https://doi.org/10.1103/PhysRevC.101.054602)
  - [28] N. Cue, Nuclear excitation by target electron capture. *Nucl. Instrum. Methods Phys. Res. B* **40-41**, 25-27 (1989). doi: [https://doi.org/10.1016/0168-583X\(89\)90914-2](https://doi.org/10.1016/0168-583X(89)90914-2)
  - [29] Z. S. Yuan, J. C. Kimball, First-principles calculation of the cross sections for nuclear excitation by electron cap-

- ture of channeled nuclei. Phys. Rev. C **47**, 323-328 (1993). doi: [10.1103/PhysRevC.47.323](https://doi.org/10.1103/PhysRevC.47.323)
- [30] A. Pálffy, W. Scheid, Z. Harman, Theory of nuclear excitation by electron capture for heavy ions. Phys. Rev. A **73**, 012715 (2006). doi: [10.1103/PhysRevA.73.012715](https://doi.org/10.1103/PhysRevA.73.012715)
- [31] A. Pálffy, J. Evers, C. H. Keitel, Isomer triggering via nuclear excitation by electron capture. Phys. Rev. Lett. **99**, 172502 (2007). doi: [10.1103/PhysRevLett.99.172502](https://doi.org/10.1103/PhysRevLett.99.172502)
- [32] Y. Wu, J. Gunst, C. H. Keitel *et al.*, Tailoring laser-generated plasmas for efficient nuclear excitation by electron capture. Phys. Rev. Lett. **120**, 052504 (2018). doi: [10.1103/PhysRevLett.120.052504](https://doi.org/10.1103/PhysRevLett.120.052504)
- [33] S. Gargiulo, I. Madan, F. Carbone, Nuclear excitation by electron capture in excited ions. Phys. Rev. Lett. **128**, 212502 (2022). doi: [10.1103/PhysRevLett.128.212502](https://doi.org/10.1103/PhysRevLett.128.212502)
- [34] Y. Wang, Z. Ma, Y. Yang *et al.*, Feasibility study of nuclear excitation by electron capture using an electron beam ion trap. Front. Phys. **11**, 1203401 (2023). doi: [10.3389/fphy.2023.1203401](https://doi.org/10.3389/fphy.2023.1203401)
- [35] Y. Yang, Y. Wang, Z. Ma *et al.*, Feasibility of probing the NEEC process using storage rings. Front. Phys. **12**, 1410076 (2024). doi: [10.3389/fphy.2024.1410076](https://doi.org/10.3389/fphy.2024.1410076)
- [36] J. Rządkiwicz, K. Słabkowska, M. Polasik *et al.*,  $^{93m}\text{Mo}$  isomer depletion via nuclear excitation by electron capture in resonant transfer into highly excited open-shell atomic states. Phys. Rev. C **108**, L031302 (2023). doi: [10.1103/PhysRevC.108.L031302](https://doi.org/10.1103/PhysRevC.108.L031302)
- [37] Z. Ma, Y. Wang, Y. Yang *et al.*, Simulation of nuclear isomer production in laser-induced plasma. Matter Radiat. Extremes **9**, 055201 (2024). doi: [10.1063/5.0212163](https://doi.org/10.1063/5.0212163)
- [38] J. Zhao, A. Pálffy, C. H. Keitel *et al.*, Efficient production of  $^{229m}\text{Th}$  via nuclear excitation by electron capture. Phys. Rev. C **110**, 014330 (2024). doi: [10.1103/PhysRevC.110.014330](https://doi.org/10.1103/PhysRevC.110.014330)
- [39] Y. Yang, H. X. Zhang, Y. B. Wu *et al.*, Physics opportunities of the nuclear excitation by electron capture process. Nucl. Sci. Tech. **36**, 17 (2025). doi: [10.1007/s41365-025-01717-0](https://doi.org/10.1007/s41365-025-01717-0)
- [40] C. J. Chiara, J. J. Carroll, M. P. Carpenter *et al.*, Isomer depletion as experimental evidence of nuclear excitation by electron capture. Nature **554**, 216-218 (2018). doi: [10.1038/nature25483](https://doi.org/10.1038/nature25483)
- [41] Y. Wu, C. H. Keitel, A. Pálffy,  $^{93m}\text{Mo}$  Isomer Depletion via Beam-Based Nuclear Excitation by Electron Capture. Phys. Rev. Lett. **122**, 212501 (2019). doi: [10.1103/PhysRevLett.122.212501](https://doi.org/10.1103/PhysRevLett.122.212501)
- [42] S. Guo, B. Ding, X. H. Zhou *et al.*, Probing  $^{93m}\text{Mo}$  Isomer Depletion with an Isomer Beam. Phys. Rev. Lett. **128**, 242502 (2022). doi: [10.1103/PhysRevLett.128.242502](https://doi.org/10.1103/PhysRevLett.128.242502)
- [43] S. G. Porsev, V. V. Flambaum, Electronic bridge process in  $^{229}\text{Th}^+$ . Phys. Rev. A **81**, 042516 (2010). doi: [10.1103/PhysRevA.81.042516](https://doi.org/10.1103/PhysRevA.81.042516)
- [44] S. G. Porsev, V. V. Flambaum, E. Peik *et al.*, Excitation of the Isomeric  $^{229m}\text{Th}$  Nuclear State via an Electronic Bridge Process in  $^{229}\text{Th}^+$ . Phys. Rev. Lett. **105**, 182501 (2010). doi: [10.1103/PhysRevLett.105.182501](https://doi.org/10.1103/PhysRevLett.105.182501)
- [45] P. V. Bilous, E. Peik, A. Pálffy, Laser-induced electronic bridge for characterization of the  $^{229m}\text{Th}$  to  $^{229g}\text{Th}$  nuclear transition with a tunable optical laser. New J. Phys. **20**, 013016 (2018). doi: [10.1088/1367-2630/aa9cd9](https://doi.org/10.1088/1367-2630/aa9cd9)
- [46] P. V. Borisyuk, N. N. Kolachevsky, A. V. Taichenachev *et al.*, Excitation of the low-energy  $^{229m}\text{Th}$  isomer in the electron bridge process via the continuum. Phys. Rev. C **100**, 044306 (2019). doi: [10.1103/PhysRevC.100.044306](https://doi.org/10.1103/PhysRevC.100.044306)
- [47] A. Y. Dzyublik, Excitation of  $^{229m}\text{Th}$  in the electron bridge via continuum, as a scattering process. Phys. Rev. C **102**, 024604 (2020). doi: [10.1103/PhysRevC.102.024604](https://doi.org/10.1103/PhysRevC.102.024604)
- [48] A. Y. Dzyublik, Quasiclassical theory of  $^{229m}\text{Th}$  excitation by laser pulses via electron bridges. Phys. Rev. C **106**, 064608 (2022). doi: [10.1103/PhysRevC.106.064608](https://doi.org/10.1103/PhysRevC.106.064608)
- [49] P. V. Bilous, H. Bekker, J. C. Berengut *et al.*, Electronic bridge excitation in highly charged  $^{229}\text{Th}$  ions. Phys. Rev. Lett. **124**, 192502 (2020). doi: [10.1103/PhysRevLett.124.192502](https://doi.org/10.1103/PhysRevLett.124.192502)
- [50] L. Li, Z. Li, C. Wang *et al.*, Scheme for the excitation of thorium-229 nuclei based on electronic bridge excitation. Nucl. Sci. Tech. **34**, 24 (2023). doi: [10.1007/s41365-023-01169-4](https://doi.org/10.1007/s41365-023-01169-4)
- [51] A. Y. Dzyublik, Photo-induced nuclear excitation by electron transition. JETP Lett. **93**, 489-494 (2011). doi: [10.1134/S0021364011090050](https://doi.org/10.1134/S0021364011090050)
- [52] A. Y. Dzyublik, General theory of nuclear excitation by electron transitions. Phys. Rev. C **88**, 054616 (2013). doi: [10.1103/PhysRevC.88.054616](https://doi.org/10.1103/PhysRevC.88.054616)
- [53] E. Tkalya, Nuclear excitation in atomic transitions (NEET process analysis). Nucl. Phys. A **539**, 209-222 (1992). doi: [https://doi.org/10.1016/0375-9474\(92\)90267-N](https://doi.org/10.1016/0375-9474(92)90267-N)
- [54] S. Sakabe, K. Takahashi, M. Hashida *et al.*, Elements and their transitions feasible for NEET. Data Nucl. Data Tables **91**, 1-7 (2005). doi: <https://doi.org/10.1016/j.adt.2005.07.002>
- [55] E. V. Tkalya, Excitation of  $^{229m}\text{Th}$  at inelastic scattering of low energy electrons. Phys. Rev. Lett. **124**, 242501 (2020). doi: [10.1103/PhysRevLett.124.242501](https://doi.org/10.1103/PhysRevLett.124.242501)
- [56] H. Zhang, W. Wang, X. Wang, Nuclear excitation cross section of  $^{229}\text{Th}$  via inelastic electron scattering. Phys. Rev. C **106**, 044604 (2022). doi: [10.1103/PhysRevC.106.044604](https://doi.org/10.1103/PhysRevC.106.044604)
- [57] B. Liu, X. Wang, Isomeric excitation of  $^{235}\text{U}$  by inelastic scattering of low-energy electrons. Phys. Rev. C **106**, 064064 (2022). doi: [10.1103/PhysRevC.106.064064](https://doi.org/10.1103/PhysRevC.106.064064)
- [58] Y. Y. Xu, J. H. Cheng, Y. T. Zou *et al.*, Inelastic-electron-scattering-induced nuclear excitation rates and dynamics in  $^{229}\text{Th}$ . Phys. Rev. C **110**, 064621 (2024). doi: [10.1103/PhysRevC.110.064621](https://doi.org/10.1103/PhysRevC.110.064621)
- [59] K. Alder, A. Bohr, T. Huus *et al.*, Errata: Study of nuclear structure by electromagnetic excitation with accelerated ions. Rev. Mod. Phys. **30**, 353 (1958). doi: [10.1103/RevModPhys.30.353](https://doi.org/10.1103/RevModPhys.30.353)
- [60] R. Hofstadter, H. R. Fechter, J. A. McIntyre, High-energy electron scattering and nuclear structure determinations. Phys. Rev. **92**, 987 (1953). doi: [10.1103/PhysRev.92.978](https://doi.org/10.1103/PhysRev.92.978)
- [61] B. Hahn, D. G. Ravenhall, R. Hofstadter, High-energy electron scattering and the charge distributions of selected nuclei. Phys. Rev. **101**, 1131 (1956). doi: [10.1103/PhysRev.101.1131](https://doi.org/10.1103/PhysRev.101.1131)
- [62] J. C. Slater, A simplification of the hartree-fock method. Phys. Rev. **81**, 385 (1951). doi: [10.1103/PhysRev.81.385](https://doi.org/10.1103/PhysRev.81.385)
- [63] F. Salvat, J. M. Fernández-Varea, radial: A Fortran subroutine package for the solution of the radial Schrödinger and Dirac wave equations. Comput. Phys. Commun. **240**, 165-177 (2019). doi: [10.1016/j.cpc.2019.02.011](https://doi.org/10.1016/j.cpc.2019.02.011)
- [64] N. Minkov, A. Pálffy, Reduced Transition Probabilities for the Gamma Decay of the 7.8 eV Isomer in  $^{229}\text{Th}$ . Phys. Rev. Lett. **118**, 212501 (2017). doi: [10.1103/PhysRevLett.118.212501](https://doi.org/10.1103/PhysRevLett.118.212501)
- [65] N. Minkov, A. Pálffy, Theoretical Predictions for the Magnetic Dipole Moment of  $^{229m}\text{Th}$ . Phys. Rev. Lett. **122**, 162502 (2019). doi: [10.1103/PhysRevLett.122.162502](https://doi.org/10.1103/PhysRevLett.122.162502)
- [66] N. Minkov, A. Pálffy,  $^{229m}\text{Th}$  isomer from a nuclear model perspective. Phys. Rev. C **103**, 014313 (2021). doi: [10.1103/PhysRevC.103.014313](https://doi.org/10.1103/PhysRevC.103.014313)



- [67] T. Kirschbaum, N. Minkov, A. Pálffy, Nuclear coherent population transfer to the  $^{229m}\text{Th}$  isomer using x-ray pulses. Phys. Rev. C **105**, 064313 (2022). [doi:10.1103/PhysRevC.105.064313](https://doi.org/10.1103/PhysRevC.105.064313)